01

X-ray diffraction in a thin crystal with non-uniform curve of reflective atomic planes

© V.I. Punegov

Institute of Physics and Mathematics of the Federal Research Center „Komi Research Center of the Ural Branch of RAS“, 167982 Syktyvkar, Russia
e-mail: vpunegov@dm.komisc.ru

Received April 2, 2024
Revised April 2, 2024
Accepted April 2, 2024

Kinematical X-ray diffraction in a curved thin crystal with depth-variable curve radius was addressed theoretically. An algorithm was developed for calculation of scattering intensity near the reciprocal lattice point from such structure using recurrent relations. Numerical simulation of X-ray diffraction in a silicon crystal was performed on four microstructure models. It is shown that reciprocal space maps of diffraction intensity distribution depend considerably on the law of crystal curve radius variation.

Keywords: kinematical X-ray diffraction, reciprocal space maps of diffraction intensity distribution, simulation of diffraction in a curved crystal.

DOI: 10.61011/TP.2024.07.58792.106-24

Introduction

Bent crystal are used for X-ray focusing [1] and spectroscopy [2], to obtain gamma-ray spectra, electron-generated high energies in curved crystals [3] and for deflection of charged high-energy particles during beam collimation in accelerators due to the channeling phenomenon [4]. Moreover, thin semiconductor crystals with non-uniform curvature are used in microelectromechanical systems, for example, in aerospace, automotive or watch-making industry [5].

X-ray diffraction is a promising method of investigation of deformed crystals, including curved periodic structures [5]. Analysis of experimental X-ray scattering data in curved crystals shall use theoretical developments. A sufficient number of theories is currently available that describe diffraction in curved crystals (see, for example, [6] and the references herein). However, numerical calculations using these theories do not agree with the experimental data. Moreover, there are no studies describing numerical calculations for reciprocal space mapping of X-ray scattering intensity from curved crystals. This is attributed to the fact that all theories are built using one-dimensional diffraction equations in terms of an incident plane X-ray wave on crystal. Actually, X-ray diffraction in the bent crystalshall be described by two-dimensional equations because the induced lattice strain is distributed both vertically and horizontally in the periodic structure. In addition, to describe diffraction in the curved crystal, a spatially constrained X-ray beam model shall be used [7,8]. The problem becomes more complicated if the crystal curvature is non-uniform in the specimen depth. Such lattice strain may be caused by crystal chip bonding to PCB [9]. This study proposes a method of calculation of reciprocal space maps (RSM) of coherent X-ray diffraction with depth-varying curve radius of reflective atomic planes.

1. X-ray diffraction in a thin crystal with variable curve of reflective atomic planes

Consider the kinematical X-ray diffraction in a thin crystal. Assume that the transverse width of the incident X-ray beam is larger than the crystal size. The objective of this study is to develop a calculation algorithm for reciprocal space mapping of X-ray scattering as applicable to the high-resolution X-ray diffraction method [10]. In the triple-axis, angular position of the sample ω and analyzer (position-sensitive detector) are related to the projections of diffraction vector deflection from a reciprocal lattice point as follows: $q_x = k \sin\theta_B(2\omega - \varepsilon)$, $q_z = -k\cos\theta_B\varepsilon$, where θ_B is the Bragg angle, $k = 2\pi/\lambda$ is the wave number, λ is the X-ray wavelength in vacuum.

First, consider the kinematical diffraction in a perfect crystal with thickness L_z and width L_x (Figure 1). An X-ray beam with size w falls on the crystal, the space (x, z) is the diffraction plane and $(L_x \cdot L_z)$ area. On the$y$ axis, the X-ray wavefront intensity is usually integrated.

Diffraction intensity distribution near a reciprocal lattice point of a perfect crystal will be written as

$$I_h(q_x, q_z) = |E_h(q_x, q_z)|^2$$

$$= |ia_h L_x L_z \operatorname{sinc}(q_x L_x/2)\operatorname{sinc}([2a_0 - q_z]L_z/2)|^2, \qquad (1)$$

where $\operatorname{sinc}(x) = \sin(x)/x$, $E_h(q_x, q_z)$ is the diffracted wave amplitude, $a_0 = \pi\chi_0/(\lambda\gamma_0)$, $a_h = C\pi\chi_h/(\lambda\gamma_{h,0})$, λ is the X-

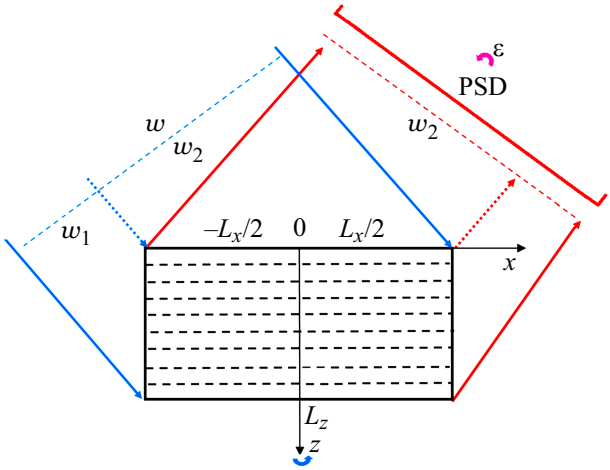

Figure 1. X-ray diffraction diagram in plane (x, z) from a perfect crystal with thickness L_z, w is the width of an X-ray beam falling on the lateral structure, lower w_1 and upper w_2 parts of the beam expose the side and surface of a crystal with size L_x. PSD — position-sensitive detector, ω and ε — crystal and detector rotations in the plane (x, z), respectively.

ray wavelength in vacuum, $\gamma_{h,0} = \sin\theta_B$, C is the polarization factor, $\chi_{0,h} = -r_0\lambda^2 F_{0,h}/(\pi V_c)$ are the Fourier components of the X-ray polarizability and $F_{0,h}$ are the structural factors in the incident and diffraction wave directions, respectively, V_c is the lattice cell volume, $r_0 = e^2/(mc^2)$ is the classical electron radius, e, m are electron charge and mass.

To describe dynamical diffraction in a strained crystal in terms of the Bragg symmetric geometry, the Takagi–Taupin equations are used [11,12]:

$$\begin{cases} (\cot\theta_B \frac{\partial}{\partial x} + \frac{\partial}{\partial z})E_0(\eta; x, z) = ia_0 E_0(\eta; x, z) \\ \quad + ia_{-h}\phi(x, z)E_h(\eta; x, z), \\ (\cot\theta_B \frac{\partial}{\partial x} - \frac{\partial}{\partial z})E_h(\eta; x, z) = i(a_0 + \eta)E_h(\eta; x, z) \\ \quad + ia_h\phi^*(x, z)E_0(\eta; x, z), \end{cases} \quad (2)$$

where $E_{0,h}(\eta; x, z)$ are transmitted and diffracted wave amplitudes, $\eta = 2k\cos(\theta_B)\omega$ is the angular parameter used in the double-crystal diffractometry in $\theta - 2\theta$ scanning mode, $k = 2\pi/\lambda$ is the wave number.

Equations (2) include a phase factor $\phi(x, z) = \exp(ihu_z(x, z))$, and the „asterisk“ means the complex conjugation, h is the reciprocal lattice vector, whereas $h = 2\pi/d_{hkl}$, where d_{hkl} is the interplanar spacing, $u_z(x, z)$ is the projection of atomic displacement vector in the reciprocal lattice vector direction.

Phase factor $\phi(x, z)$ existing in equations (2) for the bent crystalmay be written as $\phi(x, z) = \phi_x(x)\phi_z(z)$, where $\phi_x(x) = \exp(ihu_z(x))$ and $\phi_z(z) = \exp(ihu_z(z))$. Equations (2) will be rewritten as

$$\begin{cases} (\cot\theta_B \frac{\partial}{\partial x} + \frac{\partial}{\partial z})E_0(\eta; x, z) = ia_0 E_0(\eta; x, z) \\ \quad + ia_{-h}\phi_x(x)\phi_z(z)E_h(\eta; x, z), \\ (\cot\theta_B \frac{\partial}{\partial x} - \frac{\partial}{\partial z})E_h(\eta; x, z) = i(a_0 + \eta)E_h(\eta; x, z) \\ \quad + ia_h\phi^*(x)\phi_z^*(z)E_0(\eta; x, z). \end{cases} \quad (3)$$

Perform the Fourier transformation for coherent amplitudes of X-ray fields in the system of equations (3):

$$E_{0,h}(\eta; x, z) = \frac{1}{2\pi}\int_{-\infty}^{+\infty} dq_x \exp(iq_x x)\hat{E}_{0,h}(q_x, \eta; z), \quad (4)$$

where the Fourier transforms will be written as

$$\hat{E}_{0,h}(q, \eta; z) = \int_{-\infty}^{+\infty} dx \exp(-iq_x x)E_{0,h}(\eta; x, z). \quad (5)$$

Perform also the Fourier transformation for the phase factor $\phi_x(x)$:

$$\phi_x(x) = \frac{1}{2\pi}\int_{-\infty}^{+\infty} dq_x \exp(iq_x x)\phi_x(q_x), \quad (6)$$

where its Fourier transform will be written as

$$\phi_x(q_x) = \int_{-\infty}^{+\infty} dx \exp(-iq_x x)\phi_x(x). \quad (7)$$

By substituting (5) and (7) in system (3), we get Fourier domain integro-differential equations

$$\begin{cases} \frac{\partial\hat{E}_0(\kappa,\eta;z)}{\partial z} = i(a_0 - \kappa\cot\theta_B)\hat{E}_0(\kappa, \eta; z) \\ \quad + ia_{\bar{h}}\frac{\phi_z(z)\phi_x(\kappa)}{2\pi}\int_{-\infty}^{+\infty} d\kappa' \exp(i\kappa' x)\hat{E}_h(\kappa', \eta; z), \\ -\frac{\partial\hat{E}_h(\kappa,\eta;z)}{\partial z} = i(a_0 + \eta - \kappa\cot\theta_B)\hat{E}_h(\kappa, \eta; z) \\ \quad + ia_h\frac{\phi_z^*(z)\phi_x^*(\kappa)}{2\pi}\int_{-\infty}^{+\infty} d\kappa' \exp(i\kappa' x)\hat{E}_0(\kappa', \eta; z). \end{cases} \quad (8)$$

system of equations (8) describes the Fourier-domain dynamical diffraction. In case of kinematical approximation, when $a_{\bar{h}} = 0$, these equations will be written as

$$\begin{cases} \frac{\partial\hat{E}_0(q_x,\eta;z)}{\partial z} = i(a_0 - q_x\cot\theta_B)\hat{E}_0(q_x, \eta; z), \\ -\frac{\partial\hat{E}_h(q_x,\eta;z)}{\partial z} = i(a_0 + \eta - q_x\cot\theta_B)\hat{E}_h(q_x, \eta; z) \\ \quad + ia_h\phi_z^*(z)\phi_x^*(q_x)\int_{-\infty}^{+\infty} dq_x' \exp(iq_x' x)\hat{E}_0(q_x', \eta; z). \end{cases} \quad (9)$$

By substitution of the X-ray wave amplitudes

$$\begin{cases} \hat{E}_0(q_x, \eta; z) = \tilde{E}_0(q_x, \eta; z)\exp(i(a_0 - q_x\cot\theta_B)z), \\ \hat{E}_h(q_x, \eta; z) = \tilde{E}_h(q_x, \eta; z)\exp(-i(a_0 + \eta - q_x\cot\theta_B)z), \end{cases} \tag{10}$$

and using the boundary conditions

$$\hat{E}_0(\eta; x, 0) = \int_{-\infty}^{+\infty} d\kappa' \exp(i\kappa' x)\tilde{E}_0(\kappa', \eta; 0)$$

$$= \begin{cases} 1 & x \in \pm L_x/2 \\ 0 & x \notin \pm L_x/2, \end{cases}$$

where L_x is the crystal surface exposure width, system of equations (10) will be written as

$$\begin{cases} \frac{\partial \tilde{E}_0(q_x,\eta;z)}{\partial z} = 0, \\ -\frac{\partial \tilde{E}_h(q_x,\eta;z)}{\partial z} = ia_h\phi_z^*(z)\phi_x^*(q_x), \\ \exp(-i(a_0 + \eta - q_x\cot\theta_B)z). \end{cases} \tag{11}$$

According to (11), the diffraction wave amplitude equation will be written as

$$\tilde{E}_h(q_x, \eta; z) = -ia_h \int_z^0 dz'\phi_z^*(z') \times \exp(i[a_0 + \eta]z')\phi_x^*(q_x)\exp(-iq_x\cot\theta_B)z'). \tag{12}$$

Performing inverse Fourier transform (12) and considering $\phi_x^*(q_x) = \int_{-\infty}^{+\infty} dx \exp(iq_x)\phi_x(x)$, the diffraction wave amplitude depending on the spatial coordinates (x, z) may be written as an integral

$$\tilde{E}_h(q_x, \eta; z) = ia_h \int_0^z dz'\phi_z^*(z') \times \exp(i[a_0 + \eta - q_x\cot\theta_B]z') \int_{-\infty}^{+\infty} dx \exp(iq_x x)\phi_x(x). \tag{13}$$

In case of the three-crystal diffractometry, the angular variable η in the diffraction equations will be written as $\eta = q_x\cot\theta_B - q_z$, then

$$\tilde{E}_h(q_x, q_z; z) = ia_h \int_0^z dz'\phi_z^*(z') \times \exp(i[a_0 - q_z]z') \int_{-\infty}^{+\infty} dx \exp(iq_x x)\phi_x(x).$$

The expression for the intensity of a diffraction wave from a crystal with width L_x and thickness L_z is written as

$$I_h(q_x, q_z) = \left| ia_z \int_0^{L_z} dz \exp(i[a_0 - q_z)z]\phi_z(z) \times \int_{-L_x/2}^{L_x/2} dx\phi_x(x)\exp(iq_x x)\right|^2. \tag{14}$$

The field of atomic displacements of a bent crystalwill be written as

$$u_z(x, z) = u_z(x) + u_z(z), \tag{15}$$

where

$$u_z(x) = \frac{x^2}{2R}, \quad u_z(z) = \begin{cases} -\frac{\alpha}{2R}\left(z - \frac{L_z}{2}\right)^2, & z \le -\frac{L_z}{2}, \\ \frac{\alpha}{2R}\left(z - \frac{L_z}{2}\right)^2, & z > \frac{L_z}{2}, \end{cases} \text{[13].}$$

Here R is the curvature radius, constant factor α depends on the modulus of elasticity and crystal orientation. If the crystal curvature radius varies in depth of the periodic structure, then the crystal may be presented as a multilayer structure consisting of N layers. Amplitudes of the diffracted X-ray wave $E_h^N(q_x, q_z)$ from such system are calculated using a recurrent relation

$$E_h^N(q_x, q_z) = E_h^{N-1}(q_x, q_z) + \exp(iq_z L_z^{N-1})E_h^n(q_x, q_z), \tag{16}$$

where $E_h^{N-1}(q_x, q_z)$ and $E_h^n(q_x, q_z) = ia_h \int_0^{L_z^n} dz \exp[i(a_0 - -q_z)z]\phi_z^n(z) \int_{-L_x^n/2}^{L_x^n/2} dx\phi_x^n(x)\exp(iq_x x)$ — amplitudes of reflected waves from $N-1$ top layers and a bottom layer, respectively, L_z^{N-1} is the thickness of top $N-1$ layers, L_z^n is the thickness of the n-th layer. One-dimensional phase functions for the n-th layer are written as

$$\phi_x^n(x) = \exp\left[-ih\frac{x^2}{2R_n}\right]$$

and

$$\phi_z^n(z) = \exp\left[-ih\begin{cases} -\frac{\alpha}{2R_n}\left(z - \frac{L_z^n}{2}\right)^2 & z \le -\frac{L_z^n}{2} \\ \frac{\alpha}{2R_n}\left(z - \frac{L_z^n}{2}\right)^2 & z > \frac{L_z^n}{2} \end{cases}\right],$$

where R_n is the curvature radius of atomic planes of this layer.

2. Numerical simulation of X-ray diffraction mapping in a crystal with non-uniform curvature radius

The theoretical results obtained above are used to calculate the RSM for four silicon crystal microstructure models.

Different versions of curvature of reflective atomic planes in the depth of a crystal with thickness $L_z = L_{z1} + L_{z2} + L_{z3}$ are addressed, where $L_{z1,2,3}$ are the thickness of uniformly curved top part, non-uniformly curved middle and non-curved bottom part of a chip (Figure 2). Generally, the microstructure bottom may be a perfect or one-dimensionally depth-strained crystal.

Numerical calculations of the RSM are made for the microstructure models with thickness $L_z = 4\,\mu$m in case of symmetric (333) reflection ofσ-polarized X-ray Cu$K_{\alpha 1}$-radiation. The incident beam width on the lateral crystal is $w = 103\,\mu$m, whereas the bottom $w_1 = 3\,\mu$m and top $w_2 = 100\,\mu$m parts of the beam expose the side and surface of the crystal with size $L_x = 135\,\mu$m, respectively (Figure 1, 2).

The first model is the simplest for review and represents a planar perfect crystal with a constant interplanar spacing. The RSM for this model is calculated using the solution of (1). Figure 3 shows the angular distribution of X-ray scattering intensity near the reciprocal lattice from a perfect lateral crystal. The vertical band (bar) on the RSM is related to the intensity distribution of the main diffraction peak. Width of this bar depends on the lateral dimension of the crystal: the narrower the crystal the wider this bar. Periodic peaks along the vertical bar are associated with the crystal thickness. The lateral truncated low-intensity band perpendicular to the main diffraction bar is caused by the curve „tails“ of the RSM section q_x.

The second model is applicable to the uniformly bent crystalwith a curvature radius throughout the periodic structure thickness. The angular distribution of X-ray scattering intensity near the reciprocal lattice point is calculated using solution (2). Figure 4 demonstrates a calculation map from a uniformly bent crystalwith a curvature radius $R = 1$ m. Unlike the planar lateral crystal, the main diffraction peak band is broadened considerably due to the curve of the reflective atomic planes. Like for the planar crystal, the RSM exhibits an oscillatory structure along the vertical direction.

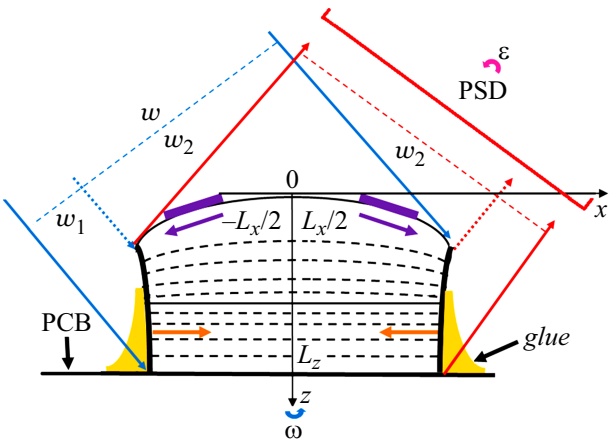

Figure 2. Schematic image of the chip in the plane (x, z) with non-uniform distribution of the reflective atomic plane curvature in the crystal depth. Here, ω and ε are crystal and detector rotations in the plane (x, z), respectively.

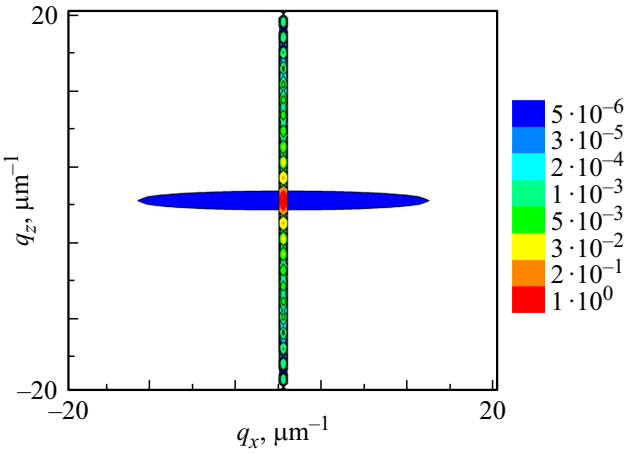

Figure 3. Calculation RSM from the planar perfect crystal with a thickness of $4\,\mu$m and surface width of$L_x = 135\,\mu$m.

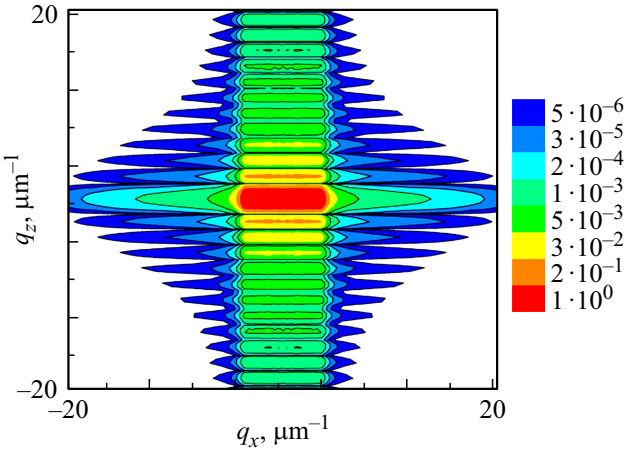

Figure 4. Calculation RSM from the uniformly bent crystalwith a thickness of $4\,\mu$m and surface width $L_x = 135\,\mu$m. Curvature radius of the reflective atomic planes $R = 1$ m.

A microstructure with a non-uniform curvature of the reflective atomic planes is described by the third model. The chip structure has the following configuration: top part of $2.5\,\mu$m in thickness, curved crystalline layer with the constant curvature radius $R = 1$ m; bottom part is a crystal structure of $1.5\,\mu$m in thickness whose curvature radius varies from 1 to 5 m. Calculation of the RSM is based on equation (2) for the top part. Then this result is fitted with the calculation of the amplitude of diffracted X-ray wave from the bottom part using recurrent equation (4). Figure 5 shows the calculation RSM from a non-uniformly bent crystalcorresponding to the third model. If for the uniformly curved structure the RSM is symmetric both vertically and laterally (Figure 4), for the case of the non-uniformly bent crystalsuch symmetry is absent (Figure 5). Calculations show that the X-ray scattering intensity distribution near

the reciprocal lattice point depends greatly on the law of curvature radius variation of the reflective atomic planes. This is demonstrated by the calculation of X-ray diffraction from a structure corresponding to the fourth model.

The fourth model is a chip with non-uniform curved top and non-curved bottom (Figure 6). The structure of such chip consists of a uniform curved upper layer of 1.75 μmin thickness with curvature radius $R = 1$ m. There is an intermediate layer of 0.25 μm in thickness where the curvature radius varies from 1 to 5 m. The chip bottom is an ideal crystal of 2 μm in thickness.

Lateral sections q_x of the RSM from the microstructure models shown above are demonstrated in Figure 7. For a perfect crystal, section q_x has a profile of a common kinematical diffraction reflection curve (curve *1*). Secondary oscillations of section q_x correspond to the crystal surface

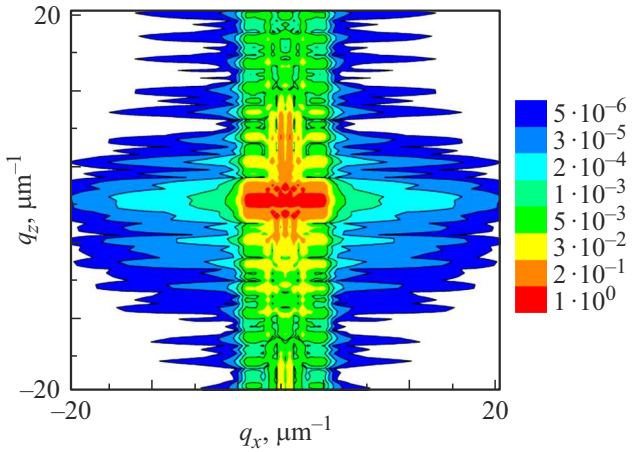

Figure 5. Calculation RSM from a non-uniformly curved crystal. The top part of 2.5 μm in thickness has a uniform curvature radius $R = 1$ m, in the bottom part of the crystal of 1.5 μm in thickness, the curvature radius varies from 1 to 5 m.

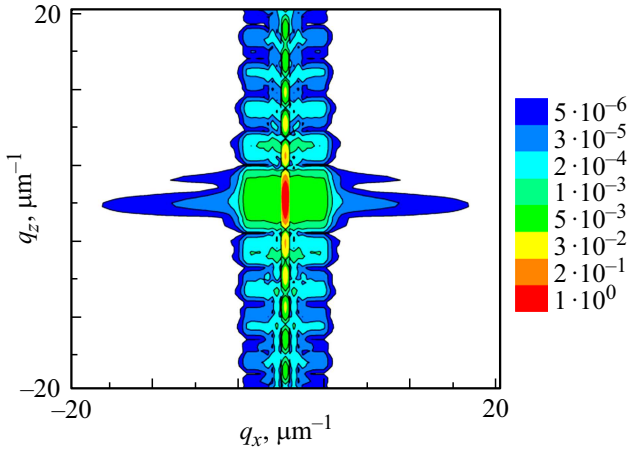

Figure 6. Calculation RSM from a crystal chip with uniformly curved top ($R = 1$ m) of 1.75 μm in thickness, the radius varies from 1 to 5 m in the middle of the crystal with a thickness of 0.25 μm, chip bottom of 2 μm in thickness corresponds to an ideal crystal.

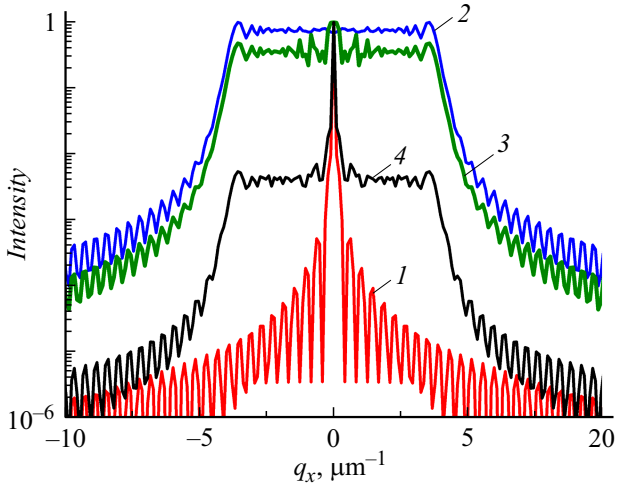

Figure 7. Calculated sections q_x-of the logarithmic RSM. Numbering of the curves corresponds to the map sections in Figure 3–6, respectively.

width, and the larger the exposed surface size the smaller the oscillation period. Curvature of the reflective planes broadens significantly the profile of section q_x (Figure 7, curve *2*). Curve *3* in Figure 7 corresponds to section q_x of the calculation RSM from the non-uniformly bent crystalwhere the top of 2.5 μm in thickness has a uniform curvature radius of $R = 1$ m, the radius varies from 1 to 5 m in the bottom of 1.5 μm in thickness. X-ray diffraction on such structure, besides a broadened profile of section q_x, is followed by the appearance of a narrow peak in the center. This is attributed to a lightly deformed region in the crystal. Calculation section q_x of the RSM from the chip with a uniformly curved top of 1.75 μm and $R = 1$ m, middle of 0.25 μm in thickness with a curvature radius varying from 1 to 5 m, and non-curved bottom of 2 μm in thickness is shown in Figure 7 (curve *4*). The presence of a layer with constant interplanar spacing in the crystal causes a narrow peak against a broadened plateau occurring due to the curved reflective atomic planes.

Figure 8 demonstrates calculated q_z (q_x) cross section the RSM from microcrystalline systems of four models. It is interesting that the profiles of sections q_z- on the RSM of the perfect and uniformly bent crystalcoincide (curves *1* and *2* in Figure 8). This is explained by the fact that the crystal is thin and the uniform bending strain has almost no effect on the atomic displacement field in the vertical direction. Non-uniform local bending strain in the crystal results in the interference of X-ray waves from various periodic structure areas, which takes a form of the curve profile of section q_z- (Figure 8, curve *3*). The presence of a planar layer that is twice as thinner broadens the diffraction reflection curve (Figure 8, curve *4*).

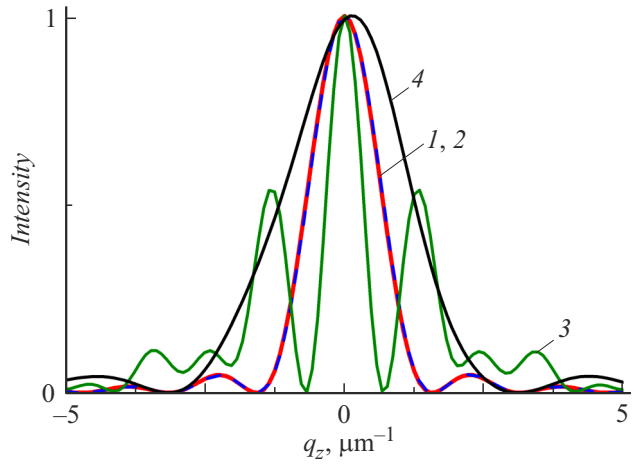

Figure 8. Calculation sections q_z- of the RSM. Numbering of the curves corresponds to the map sections in Figure 3−6, respectively.

Conclusion

The study uses a kinematical solution to perform numeric simulation of X-ray diffraction mapping from crystalline silicon chips with various configurations. All calculations have been made for laterally limited crystals being „awash“ in the X-ray beam, i.e. both the side and top of the chip are exposed. Since analytical solution (1) is used for the perfect crystal, it takes about 1 s to calculate the RSM using a „Intel CORE i7-7740X“ PC, and it takes from 2 to 5 min to calculate the intensity of X-ray scattering from the bent crystal using solution (2). On the other hand, numeric solutions using nodal grids [14] on the basis of the Takagi−Taupin equations or two-dimensional recurrent relations with the same accuracy are performed within 1 h.

Conflict of interest

The author declares that he has no conflict of interest.

Funding

The study was supported financially by grant № 23-22-00062 provided by the Russian Science Foundation, https://rscf.ru/project/23-22-00062/

References

[1] Y.I. Nesterets, S.W. Wilkins. J. Appl. Cryst., **41**, 237 (2008). DOI: 10.1107/S0021889808000617
[2] D. Zhu, M. Cammarata, J.M. Feldkamp, D.M. Fritz, J.B. Hastings, S. Lee, H.T. Lemke, A. Robert, J.L. Turner, Y. Feng. Appl. Phys. Lett., **101**, 034103 (2012). http://dx.doi.org/10.1063/1.4736725
[3] L. Bandiera, A. Sytov, D. De Salvador, A. Mazzolari, E. Bagli, R. Camattari, S. Carturan, C. Durighello, G. Germogli, V. Guidi, P. Klag, W. Lauth, G. Maggioni, V. Mascagna, M. Prest, M. Romagnoni, M. Soldani, V.V. Tikhomirov, E. Vallazza. Eur. Phys. J. C, **81**, 284 (1−9) (2021). DOI: 10.1140/epjc/s10052-021-09071-2
[4] R. Camattari, M. Romagnoni, L. Bandiera, E. Bagli, A. Mazzolari, A. Sytov, S. Haaga, M. Kabukcuoglu, S. Bode, D. Hänschke, A. Danilewsky, T. Baumbach, V. Bellucci, V. Guidia, G. Cavoto. J. Appl. Crystallogr., **53**, 486 (2020). DOI: 10.1107/S1600576720002800
[5] A. Neels, A. Dommann. Techn. Proc. NSTI-Nanotech, **2**, 182 (2010).
[6] A.-P. Honkanen, C. Ferrero, J.-P. Guigay, V. Mocella, J. Appl. Cryst., **51**, 514 (2018). https://doi.org/10.1107/S1600576718001930
[7] V.I. Punegov, K.M. Pavlov, A.V. Karpov, N.N. Faleev. J. Appl. Cryst., **50**, 1256 (2017). DOI: 10.1107/S1600576717010123
[8] V.I. Punegov, S.I. Kolosov, K.M. Pavlov. J. Appl. Cryst., **49**, 1190 (2016). DOI: 10.1107/S1600576716008396
[9] A. Neels, G. Bourban, H. Shea, A. Schifferle, E. Mazza, A. Dommann. Proced. Chem., **1**, 820 (2009). DOI: 10.1016/j.proche.2009.07.204
[10] V.I. Punegov. Physics−Uspekhi, **58**, 419 (2015). DOI: 10.3367/UFNr.0185.201505a.0449
[11] S. Takagi. Acta Cryst., **15**, 1311 (1962).
[12] D. Taupin. Bull. Soc. Fr. Miner. Crist., **87**, 469 (1964).
[13] T. Fukamachi, S. Jongsukswat, D. Ju, R. Negishi, K. Hirano, T. Kawamura. Acta Cryst. A, **75**, 842 (2019). DOI: 10.1107/S2053273319011859
[14] V.I. Punegov, S.I. Kolosov. J. Appl. Cryst., **55**, 320 (2022). DOI: 10.1107/S1600576722001686

Translated by E.Ilinskaya